D. André d'Avignon[1]
G. Larry Bretthorst[1]
Marilyn Emerson Holtzer[1]
Kathleen A. Schwarz[1]
Ruth Hogue Angeletti[2]
Lisa Mints[2]
Alfred Holtzer[1]
[1] *Department of Chemistry, Washington University, Campus Box 1134, One Brookings Drive, St. Louis, MO 63130-4899*

[2] *Laboratory for Macromolecular Analysis & Proteomics, Albert Einstein College of Medicine, 1300 Morris Park Avenue, Bronx, NY 10461*

Site-Specific Experiments on Folding/Unfolding of Jun Coiled Coils: Thermodynamic and Kinetic Parameters from Spin Inversion Transfer Nuclear Magnetic Resonance at Leucine-18

Received 2 February 2006; revised 31 May 2006; accepted 6 June 2006
Published online 9 June 2006 in Wiley InterScience (www.interscience.wiley.com). DOI 10.1002/bip.20555

Abstract: *The 32-residue leucine zipper subsequence, called here Jun-lz, associates in benign media to form a parallel two-stranded coiled coil. Studies are reported of its thermal unfolding/folding transition by circular dichroism (CD) on samples of natural isotopic abundance and by both equilibrium and spin inversion transfer (SIT) nuclear magnetic resonance (NMR) on samples labeled at the leucine-18 α-carbon with 99% ^{13}C. The data cover a wide range of temperature and concentration, and show that Jun-lz unfolds below room temperature, being far less stable than some other leucine zippers such as GCN4. ^{13}C-NMR shows two well-separated resonances. We ascribe the upfield one to ^{13}C spins on unfolded single chains and the downfield one to ^{13}C spins on coiled-coil dimers. Their relative intensities provide a measure of the unfolding equilibrium constant. In SIT NMR, the recovery of the equilibrium magnetization after one resonance is inverted is modulated in part by the unfolding and folding rate constants, which are accessible from the data. Global Bayesian analysis of the equilibrium and SIT NMR data provide values for the standard enthalpy, entropy, and heat capacity of unfolding, and show the latter to be unusually large. The CD results are compatible with the NMR findings. Global Bayesian analysis of the SIT NMR data yields the corresponding activation parameters for unfolding and folding. The results show that both reaction directions are activated processes. Activation for unfolding is entropy driven, enthalpy opposed. Activation for folding is strongly enthalpy opposed and somewhat entropy opposed, falsifying the idea that the barrier for folding is solely due to a purely entropic search for properly reg-*

Correspondence to: Alfred Holtzer; e-mail: Holtzer@wustl.edu
Contract grant sponsor: Washington University Mass Spectrometry Resource, a National Institutes of Health Research Resource; contract grant number: P41RR0954

istered partners. The activation heat capacity is much larger for folding, so almost the entire overall change is due to the folding direction. This latter finding, if it applies to GCN4 leucine zippers, clears up an extant apparent disagreement between folding rate constants for GCN4 as determined by chevron analysis and NMR in differing temperature regimes. Biopolymers 83: 255–267, 2006

This article was originally published online as an accepted preprint. The "Published Online" date corresponds to the preprint version. You can request a copy of the preprint by emailing the Biopolymers editorial office at biopolymers@wiley.com

Keywords: *leucine zipper; protein folding; protein denaturation; spin inversion transfer; coiled coils*

INTRODUCTION

The α-helical coiled coil is a protein fold originally discovered in certain long fibrous proteins, such as tropomyosin and paramyosin.[1] They are examples of the simplest coiled coils, in which two α-helical peptide chains are arranged in parallel and register and slightly supertwisted, and are particularly attractive subjects of physical study because of their structural simplicity. The structure is based on a pseudo-repeating heptad of amino acids, designated *abcdefg*, in which residues *a* and *d* are hydrophobic and *e* and *g* are usually oppositely charged.[2,3]

More recently, the coiled-coil motif has been found to be common in many globular proteins as well.[1] Some shorter coiled coils, subsequences of larger proteins, are stable by themselves. These have leucine residues at the *d* heptad position, are called leucine zippers, and have been much studied.[4–8] However, only a limited number of appropriate sequences have been subjected to detailed thermodynamic and kinetic analysis of their folding/unfolding transitions. For example, although the coiled-coil, leucine-zipper region of the GCN4 transcription factor, called here GCN4-lz, has been extensively studied,[9–13] the Jun coiled coil, which was also discovered early on,[14,15] has not. As a result, in spite of considerable effort, no overarching physical model for the folding/unfolding of two-chain coiled coils has gained general acceptance.

Here, we attempt to remedy this situation by circular dichroism (CD) and nuclear magnetic resonance (NMR) studies of the thermal conformational transition of a dimeric Jun coiled coil. In the transition primarily studied here, the two strands are not cross-linked, so a folded dimeric coiled coil converts to two unfolded monomer chains. CD is useful for learning general features of the transition, but quantitative interpretation is difficult, because CD measures the helix content averaged over all peptide groups in the molecular ensemble. The difficulty is that the dimers are likely to be less than fully helical and the monomers less than fully random. It is therefore not known what the temperature dependence of the mean residue ellipticity of the dimer or monomer ensembles might be. A function of unknown form is more difficult to evaluate than a constant parameter.

NMR, on the other hand, is site specific. By choosing to label the Jun peptide backbone at a $^{13}C^{\alpha}$ near the middle of the chain, we can be confident, after suitable tests of the results for self-consistency, that the upfield resonance is due to unfolded monomer chains and the downfield resonance to folded dimers, provided that the interconversion is slow on the NMR time scale. Equilibrium studies of the relative resonance intensities thus provides a measure of the weight fraction of monomer (g_m), which, along with the total peptide-chain formality (C_0) provides the dimer–monomer equilibrium constant. That is, for the unfolding reaction,

$$F = 2U \tag{1}$$

wherein F represents the ensemble of folded dimers and U that of unfolded monomers, we have

$$K_{eq} = (2C_0 {g_m}^2)/(1 - g_m). \tag{2}$$

The equilibrium constant is connected to other thermodynamic properties via

$$\begin{aligned}[-\Delta G^{\infty}(T)/RT] = \ln K_{eq}(T) = [-\Delta H^{\infty}(T_0)/RT] \\ + [\Delta S^{\infty}(T_0)/R] + [\Delta C_P^{\infty}/R] \\ \times [(T_0/T) - 1 - \ln(T_0/T)]\end{aligned} \tag{3}$$

wherein the standard Gibbs energy, entropy, and constant-pressure heat capacity changes are given their usual symbols, and T_0 represents any suitable reference temperature, taken here as 285 K, i.e., 11.85°C.

Moreover, in spin inversion transfer (SIT) experiments, in which an inversion pulse is specifically

tuned to either the upfield or the downfield resonance, the time course of the recovery of the Z component of magnetization is modulated by the folding and unfolding rates as well as by the spin–lattice relaxation rate of each species, and all four rate constants can be teased out of the free induction decay (FID) data.[16,17] Analysis of the SIT results can provide the thermodynamic characteristics of the equilibrium (standard enthalpy, entropy, and heat capacity) and the corresponding activation parameters for both reaction directions. The latter are obtained via the usual kinetic Eyring model:

$$F = A^{\ddagger} = 2U \tag{4}$$

wherein $A^{\ddagger}$ represents the transition state ensemble. Eyring's theory gives for the rate constant for either direction:

$$\ln k_i = \ln Z - [\Delta H_i^{\ddagger}(T_0)/RT] + [\Delta S_i^{\ddagger}(T_0)/R] + [\Delta C_{P,i}^{\ddagger}/R][(T_0/T) - 1 - \ln(T_0/T)] \tag{5}$$

wherein Z is the Eyring preexponential factor for which we use the compromise value 10^{10} s^{-1}, and the subscript i represents "unf" for the forward direction of reaction equation (4) and "fld" for the reverse. This compromise choice of Z has been discussed earlier.[13] It affects only the value of the activation entropy. No other choice within the reasonable range would change our conclusions.

Below, we report such thermodynamic and kinetic values for a Jun coiled coil. In particular, we choose the natural abundance sequence previously called JunN by Kim and coworkers,[15] but we omit the CGG tripeptide at the N-terminus. We designate our peptide Jun-lz. This Jun peptide differs slightly in sequence from the peptide used in earlier work from the Kim lab that was designated Jun-p1N.[14] Our NMR-labeled version of Jun-lz has the sequence Ac-IARLEEK VKTLKAQ NYE**L**AST ANMLREQ VAQL-Am, wherein residue L-18 is underlined to indicate that it bears 99% ^{13}C at the α-carbon. Note that both ends of the chain are capped, and the 32-residue sequence is presented in heptads, starting with the N-terminal isoleucine, which is an *a* residue in the signature heptad that characterizes coiled-coil sequences.[3] Note, too, that all *d* residues are leucines, so this is indeed a "leucine zipper" sequence. We designate this labeled peptide Jun-lz-L18, but its conformational equilibria are indistinguishable from its natural abundance counterpart.

Although our primary interest here is in the dissociating unfolding transition undergone by this peptide, a few CD experiments are also reported on a related sequence, differing only by having natural abundance carbon at L18 and insertion of a CGG sequence between the acetyl cap and the N-terminal isoleucine residue. This allows covalent linkage of the two strands via a disulfide bridge. We refer to the cross-linked form of this natural abundance peptide as $(CGG\text{-}Jun\text{-}lz)_2$.

As will be seen below, the folding/unfolding process in the noncross-linked Jun-lz-L18 peptide contrasts in many respects from the corresponding characteristics shown by previous studies of GCN4-like peptides.[9–13] Jun-lz's coiled coil is far less stable than GCN4's, and the thermodynamic parameters characterizing both the equilibrium and kinetic activation are quite different in the two peptides. However, certain features are seen to be held in common, once one corrects for the vastly different temperature regimes in which they unfold. Further insight can doubtless be gained into the molecular nature of the dimer and monomer ensembles by study of peptides with $^{13}C^{\alpha}$ labels at other sites, particularly those distant from the center of the chain, as has been reported for the GCN4-lzK peptide.[18,30] Indeed, such studies have begun here, but are at a preliminary stage.

MATERIALS AND METHODS

Peptide Synthesis, Purification, and Analyses

The Jun-lz peptides were made by solid-phase synthesis using the same techniques as previously described for the GCN4 leucine-zipper (GCN4-lz) peptide.[13] The 99% $^{13}C^{\alpha}$-labeled 9-fluorenylmethoxycarbonyl (Fmoc) leucine was also prepared as in prior work.[18] Analytical high performance liquid chromatography (HPLC) was used after each NMR and CD experiment to check for sample damage.

Purification was effected via reversed-phase HPLC using a Beckman system equipped with a Vydac preparative column for polypeptides (C18, 22 × 250 mm) as previously described.[16] Purity was assessed via analytical reversed-phase HPLC (Vydac C18, 4 × 250 mm) and only those fractions having at least 97% purity were used for the physical measurements. Cross-linkable CGG-Jun-lz was purified similarly, but in two successive HPLC steps. First, any existing disulfide cross-links were reduced by heating the crude material to 55°C for 5 min in $(NaPi)_{50}(DTT)_{10}(7.4)$ (DTT: dithiothreitol). We designate complex aqueous solvents by listing each constituent (except water) with a subscript giving its millimolarity, followed by the pH in parentheses. Analytical HPLC allowed selection of those fractions having purity greater than 90%. Second, the selected fractions were air oxidized to produce

$(CGG\text{-}Jun\text{-}lz)_2$ by stirring overnight at room temperature in $(NH_4HCO_3)_{100}(7.9)$, and subsequently brought to 97% purity by further HPLC.

The molecular masses of the purified peptides were determined by mass spectrometry and found to be within 1 Da of the expected values: 3701.3 for Jun-lz (natural abundance); 3702.3 for Jun-lz-L18; and 3918.6 for reduced CGG-Jun-lz (natural abundance).

Peptide concentration was measured via UV absorbance at 275 nm, using a tyrosine extinction coefficient of 1.40 mM^{-1} cm^{-1}. Because there is only one tyrosine per chain, this provides the total formality of peptide chains as well. Extinction coefficients for both natural abundance Jun-lz and Jun-lz-L18 were determined by a modification[19] of the Edelhoch method.[20] The same value was assumed for $(CGG\text{-}Jun\text{-}lz)_2$.

Circular Dichroism

A Jasco (Easton, MD) J500A spectropolarimeter equipped with a Jasco IF-500 interface was used for the CD measurements. Procedures for the acquisition of digitized CD data and subsequent analysis thereof have been described.[21] CD unfolding curves were found to be the same for natural abundance and labeled Jun-lz samples of the same concentration. The solvent for all physical studies, CD and NMR, reported here is $(NaCl)_{100}(NaPi)_{50}(7.4)$.

Nuclear Magnetic Resonance

Both equilibrium and SIT NMR measurements were made as previously described[16] with the following exceptions. For the equilibrium measurements, 2000 transients were collected with a 3-s relaxation delay. In this study, we alternated the proton-decoupling field from on resonance during acquisition to 100 kHz (200 ppm) off resonance during the equilibration period. This strategy was adopted because in preliminary studies we found that the observed fraction monomer differed by a small amount ($\sim$3%), depending on the presence or absence of the decoupling field. We ascribe this discrepancy to different Overhauser enhancements between the resonances of the folded and unfolded forms, which have different rotational correlation times. Because both on- and off-resonance fields were only 2-kHz (4 ppm) wide, the 100-kHz shift off resonance removes any influence of differential Overhauser enhancements. The adopted protocol therefore not only vitiates the effects of differing Overhauser enhancements, but because the decoupling field is never entirely off, our temperature calibration is not compromised. The SIT experiments employed a Gaussian pulse of 15-ms duration and data from 1120 transients were recorded for 16 delay times from 0 to 2 s after inversion.

In some of the NMR experiments, a small amount of a wispy material was seen in the solution near the Shigemi insert when the NMR tube was removed. Remeasurement of the spectrum at a temperature already employed gave precisely the same results as those obtained originally, and subsequent HPLC analysis showed no sample damage. Centrifugation of the recovered sample yielded no palpable pellet, and the ultraviolet (UV) absorption of the supernatant was unchanged from that found prior to the NMR experiment. We have no cogent explanation for this observation, but its effect on the results is apparently nil.

Bayesian Analyses

Analysis of the NMR Data. NMR data in both the equilibrium and SIT experiments consist of FIDs, each at a given measured temperature and concentration. In addition, a FID from the SIT experiment has a particular delay time associated with it. The concentration is measured rather precisely, and was therefore assumed known. Prior experience with such data in which we allowed this quantity to vary showed no improvement in the results, justifying this choice. Temperature measurement in NMR, however, is uncertain to within about one degree, and, being a more influential variable, was allowed to vary in the simulations used to evaluate the joint posterior probability for the various parameters. This allows the Bayesian procedure to choose the best temperature within those limits.

As noted above, the important quantities are the relative intensities of the monomer and dimer resonances, which provide the fraction monomer, g_m, and its dimer counterpart, $g_d = 1 - g_m$. These were estimated using Bayesian probability theory,[22–26] and these estimated intensities are used in the analysis. They are related to the thermodynamic properties through Eqs. (1)–(5).

For the equilibrium NMR measurements, for example, we designate the measured equilibrium magnetization of the monomer as $D_m^\infty(T_i,C_j) = M^\infty\, g_m(T_i,C_j) + n_m^\infty$, in which M is the total equilibrium magnetization and n_m^∞ is the uncertainty in the measurement. The analogous expression is used for the dimer species. Each equilibrium data set has one total magnetization and the individual species magnetizations must obey the equilibrium condition $M_m^\infty / M_d^\infty = g_m/g_d$.

The SIT data comprise a series of inversion-recovery FIDs in which either the monomer or dimer resonance is selectively inverted initially. A total of 16 different SIT data sets was acquired at various temperatures and concentrations. Each set comprises 14 or 16 FIDs at varying delay times. For a given set, the monomer and dimer resonance intensities are obtained via solution of the magnetization exchange equations,[16] providing a rate constant for each direction of reaction. One must recognize here that the SIT technique can only yield a rate constant for spin exchange, i.e., for the reaction[13,16,17]

$$a \rightleftharpoons b \tag{6}$$

wherein a represents a ^{13}C spin in an environment characteristic of the folded ensemble and b a spin in an environment characteristic of the unfolded ensemble. The rate constants for these transformations, k_{ab} and k_{ba} are the ones determined in the SIT experiment. These are related to the chemical rate constants applicable to reaction Eqs. (1) and (4) by[13,16,17]

$$k_{\text{unf}} = k_{ab} \tag{7}$$

$$k_{\text{fld}} = [k_{ba}(k_{ab} + k_{ba})]/[2C_0 k_{ab}]. \tag{8}$$

The equilibrium constant is related to these by

$$K_{\text{unf}} = k_{\text{unf}}/k_{\text{fld}} = [2C_0 {k_{ab}}^2]/[k_{ba}(k_{ab} + k_{ba})] \tag{9}$$

and the weight fraction monomer is

$$g_{\text{m}} = k_{ab}/(k_{ab} + k_{ba}) \tag{10}$$

The chemical rate constants are related to the Eyring activation parameters through Eq. (5). The same equilibrium condition applies in the SIT experiments in the long-time limit as for the equilibrium measurements.

In the SIT case, there are additional parameters in the initial longitudinal magnetizations, i.e., right after the inversion pulse, M_{m}^0, M_{d}^0, and their sum, M^0. Furthermore, in addition to these reaction kinetic parameters, the recovery of longitudinal magnetization is also modulated by the values of the longitudinal relaxation times, $T_{1\text{m}}$ and $T_{1\text{d}}$. These relaxation times are also dependent on temperature. We approximate that dependence via

$$T_{1i} = T_{1i}^{\infty} + [\Delta T_{1i}^{\infty} \eta(T)/T] \tag{11}$$

wherein T_{1i}^{∞} is the value of T_{1i} at very high temperature, subscript i is either "m" or "d," ΔT_{1i}^{∞} is a slope, and $\eta(T)$ is the viscosity of solvent at T, for which we used the viscosity of water.

All NMR data sets, equilibrium, and SIT, are assumed to be independent. Consequently, the likelihood for all data is the product of the likelihoods for each separate set. These likelihoods were assigned using Gaussians with known standard deviations for each value. The prior probability for the amplitudes were assigned using broad, uninformative Gaussian prior probabilities. The prior probabilities for all of the thermodynamic variables were assigned using bounded Gaussians. These bounds were wide, and served mainly to inform the numerical simulations of the order of magnitude of the parameters.

The sum rule of probability theory was applied to the joint posterior probability for both the amplitudes and the thermodynamic parameters to remove the amplitudes. The process, called "marginalization," results in a joint posterior probability containing only the thermodynamic parameters. A Metropolis–Hastings Markov Chain Monte Carlo (MCMC) simulation[27–29] was performed to approximate the Bayesian joint posterior probability for the thermodynamic parameters. The resulting parameter samples were used to generate all of the plots from the NMR data presented below.

Analysis of the CD Data. The CD data comprise 10 different measurements of thermal unfolding at concentrations varying from 5.33 to 1200 μM. Each set has 18–36 values of the mean-residue ellipticity at 222 nm with temperatures ranging from roughly 1 to 57°C. According to the model of Eq. (1), each measured mean-residue ellipticity at 222 nm would be a simple weighted function of two concentration-independent functions of T, the mean-residue ellipticity at 222 nm of monomers, $[\Theta_{\text{m}}(T)]$, and of dimers, $[\Theta_{\text{d}}(T)]$. That is,

$$[\Theta(T, C_0)] = g_{\text{m}}(T, C_0)[\Theta_{\text{m}}(T)] + g_{\text{d}}(T, C_0)[\Theta_{\text{d}}(T)]. \tag{12}$$

All that is needed in the Bayesian analysis is to add to the right-hand side a term recognizing that there is some error in the measurement.

Parameters that are to be inferred in the analysis are the standard enthalpy, entropy, and heat capacity changes of Eq. (3), from which g_{m} may be computed, and the mean residue ellipticities of the monomer and dimer species. The latter two functions were discretized at integral temperatures from zero to 59°C and linear interpolation used for temperatures in between. Consequently, there are 123 parameters [*sic!*] to estimate from the CD data.

Again, Bayesian probability theory was used to obtain the joint posterior probability for these parameters. This joint posterior probability was factored into independent prior probabilities for the thermodynamic parameters and these priors were assigned using bounded Gaussians that simply specify the order of magnitude of each. The prior probabilities for the discretized functions were assigned using a correlated prior probability that constrained the first derivatives of these functions. This prior imposed a smoothness condition on these functions. Finally, the likelihood for the CD data was assigned using a Gaussian prior for the noise with an unknown standard deviation. The rules of probability theory were used to remove the noise standard deviation and the resulting marginal probability was of the form of Student's t-distribution.

A MCMC simulation was then used to approximate the joint posterior probability for the parameters.[27–29] Samples from these simulations provided estimates for all of the model's parameters and functions.

Needless to say, there are difficulties with such an analysis. The number of parameters is large, and our ignorance of the functional form of the temperature-dependent ellipticities for monomer and dimer is a serious drawback. In the case of GCN4-like leucine zippers, for example, there is ample evidence that neither the dimer nor the monomer ensemble is conformationally uniform.[16–18,30,31] The Jun-lz dimer may contain transient unfolded regions and the monomer transient folded regions that are temperature sensitive. Moreover, either or both may "cold denature," leading to individual unfolding curves that may not be monotonic. Consequently, the results of the analysis of the CD are merely approximate. Nevertheless, our findings are reported below and compared with the ones from NMR.

RESULTS

General Features of the Transition from CD and NMR

General Features of the Transition from CD. CD in the backbone region is the canonical choice for an

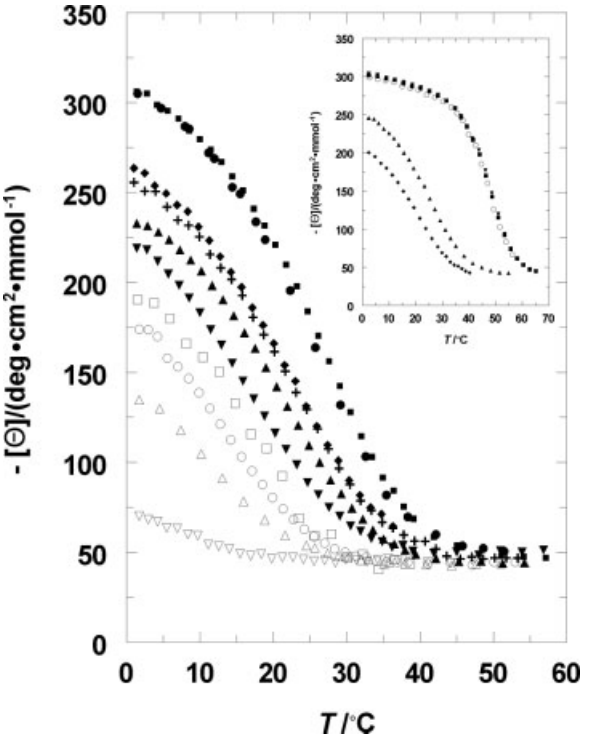

FIGURE 1 Negative of the mean-residue ellipticity at 222 nm vs. temperature for Jun-lz in $(NaCl)_{100}(NaPi)_{50}(7.4)$. Concentrations ($\mu M$) are, from top down: 1200, 1080, 637, 631, 358, 181, 88.5, 61.0, 30.0, 5.3. Inset: upper curve, cross-linked at N-terminus (see text), for which concentrations (μM) are: filled squares, 1040; filled dels, 257; open circles, 7.9. Inset: lower two curves are re-reduced; upper curve, 1040 μM; lower curve, 333 μM.

overview of protein folding/unfolding transitions, because it reports on every peptide bond in the molecule. Figure 1 shows our data for thermal unfolding of the natural abundance Jun-lz peptide at various peptide formalities (as monomer) ranging from 5.3 to 1200 μM in the saline buffer $(NaCl)_{100}(NaPi)_{50}(7.4)$. These thermal curves are completely reversible, so it is the equilibrium population that is reflected in these data. As expected for a two-stranded, noncross-linked dimer, the unfolding transition's midpoint temperature decreases markedly with dilution. It is also apparent that the folded dimer is far less stable thermally than its GCN4-lz counterpart,[13] with Jun-lz unfolding at temperatures some 50°C lower at comparable concentrations.

One other feature of these data differentiates Jun-lz from other coiled coils. In most coiled coils, the negative of the ellipticity shows a pronounced linear decline with increasing temperature, followed by a more cooperative fall.[32] The latter signifies the dissociation of the chains.[33] In Jun-lz, the initial linear portion is absent. Instead, whatever the concentration, the curves all approach a maximum as temperature drops toward zero. This feature strongly suggests that Jun-lz would undergo "cold denaturation" if one could access the temperature range below the freezing point of the aqueous solvent. This, in turn, implies that Jun-lz has a larger standard heat capacity change with unfolding than other coiled coils examined hitherto. As is seen below, this feature is corroborated by our NMR studies. Our Bayesian analysis of these CD unfolding curves will be discussed below after consideration of the NMR results.

Because it is always wise to be sure that protein aggregation above the dimer level is absent, a CD study was carried out of the cross-linked, natural abundance $(CGG\text{-}Jun\text{-}lz)_2$ peptide. Our CD data for this disulfide-cross-linked form appears in the Figure 1 inset for concentrations varying from 7.3 to 1037 μM. As can be seen, this peptide, in which dissociation to monomer chains cannot occur, unfolds at a much higher temperature than its noncross-linked counterpart, as expected. However, there is no concentration dependence, so there is no apparent tendency for Jun-lz to aggregate beyond the dimer level. The melting temperature of $(CGG\text{-}Jun\text{-}lz)_2$ is $\sim 47°C$, in good agreement with the value of 41°C found in the Kim lab[15] employing a medium of lower ionic strength, i.e., $(NaCl)_{50}(NaPi)_{10}(7.0)$. The Figure 1 inset also shows that reduction of the disulfide, by addition of DTT to the cross-linked dimer, restores the temperature sensitivity and concentration dependence characteristic of the noncross-linked version.

General Features of the Transition from Equilibrium NMR. A sampling of our ^{13}C-NMR spectra for Jun-lz-L18 is given in Figure 2, from which the trends with temperature (A) and concentration (B) can be seen. Two features are immediately obvious. First, only two rather widely separated resonances appear, indicating two different magnetic environments in slow exchange and making it possible to measure their relative populations from their relative resonance intensities. This observation, coupled with Occam's razor, immediately suggests a two-state model for the equilibrium conformational population. Because the $^{13}C^{\alpha}$-label is near the middle of the peptide chain, we interpret the upfield resonance as from the ensemble of separated monomer chains and the downfield resonance as from the ensemble of folded dimers. This allows conversion, via Eq. (2), of the relative populations into an equilibrium constant for the reaction represented in Eq. (1). Second, the trends seen with temperature and concentration are consistent with this view: Increasing T or dilution augment the intensity of the upfield resonance. More quantita-

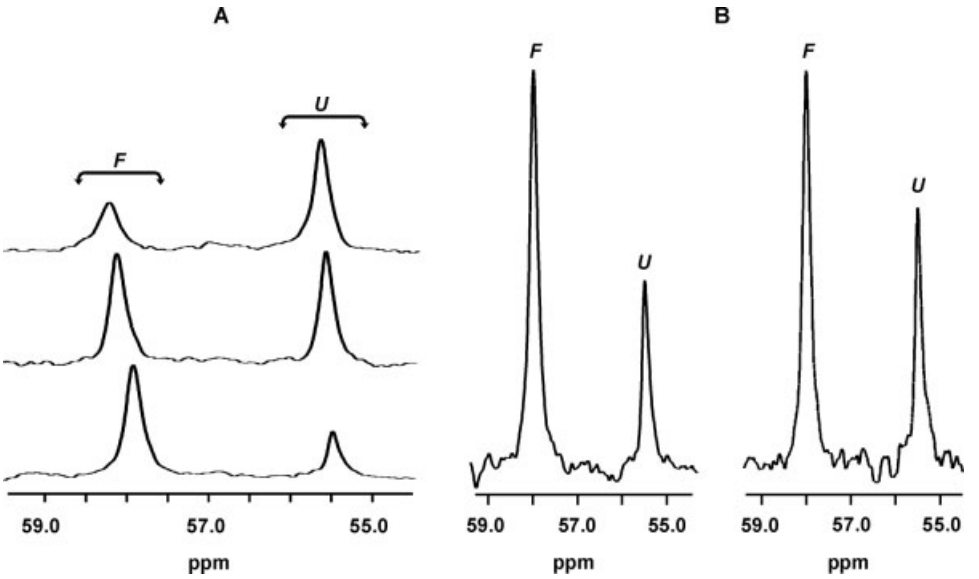

FIGURE 2 $^{13}C^{\alpha}$-NMR spectra of Jun-lz-L18 in $(NaCl)_{100}(NaPi)_{50}(7.4)$ as function of temperature and concentration. (A) All at a concentration of 1166 μM. Temperatures (°C) from top down: 23.9, 16.3, 1.88. (B) All at a temperature of 7.63°C. Left spectrum, 1310 μM; right spectrum, 816 μM. Solvent is as in Figure 1.

tive demonstration of the self-consistency of this interpretation is given below.

General Features of the Transition from SIT NMR. Sample SIT spectra are shown in Figure 3. It is immediately obvious from these that the two resonances are undergoing chemical exchange. For example, the inverted resonance of the folded form (Figure 3A) rises to its equilibrium value in time, as expected. Were the two not in exchange, the noninverted resonance of the unfolded form would simply remain at equilibrium in the applied magnetic field. Instead, it first declines in intensity, as unfolded chains convert to the folded form, bringing their inverted spins with them, then it eventually rises to the appropriate equilibrium value. Figure 3B shows a similar effect when the unfolded form is inverted.

The reader is reminded that only spins are manipulated in the SIT experiment; the conformational equilibrium is never disturbed.[16,17] Figure 3 therefore provides a graphic demonstration that Eq. (1) describes a mobile equilibrium. This also means that rate constants are measured at equilibrium, not as one approaches it, which is more common. It is a long-standing tenet of physical chemistry, of course, that the rate constants depend only on T, not on the proximity of the system to equilibrium.

Figure 4 shows the contribution of each resonance to the longitudinal magnetization as function of time. The recovery of magnetization is modulated by the normal relaxation rate of each resonance (its $R_1 = 1/T_1$ value) and by the rate constants for the unfolding and folding transitions, all of which can be teased out of the data.[16,17] Results of global Bayesian analysis

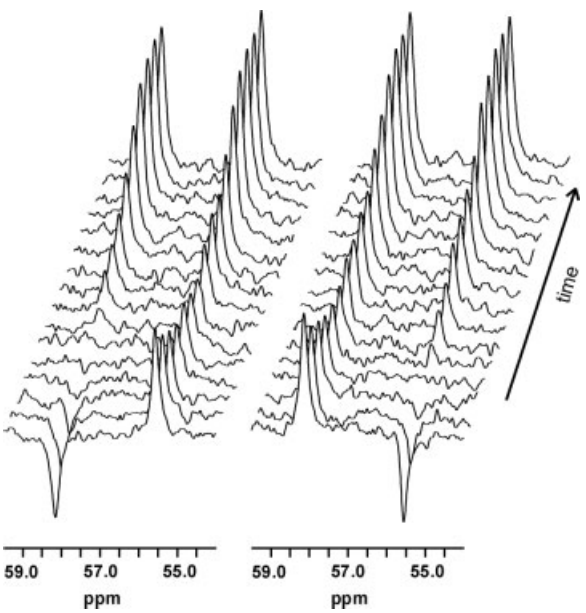

FIGURE 3 SIT NMR inversion-recovery experiment. Jun-lz-L18 concentration is 1310 μM at 18.2°C. Left spectra, folded form (downfield resonance) initially inverted; right spectra, unfolded form (upfield resonance) initially inverted. Delay times: 0.0 (just after inversion), 0.01, 0.02, 0.03, 0.04, 0.06, 0.08, 0.12, 0.16, 0.20, 0.30, 0.50, 0.80, 1.2, 1.6, 2.0 s. Solvent is as in Figure 1.

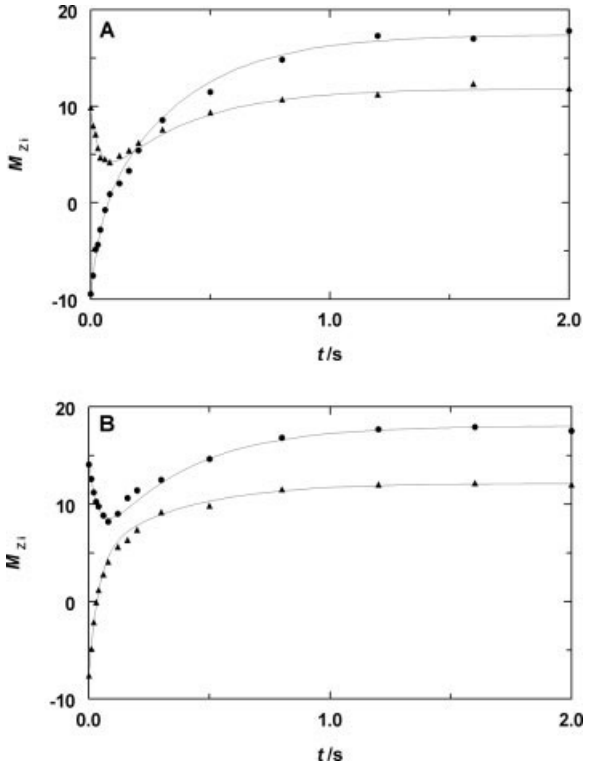

FIGURE 4 Time course of longitudinal magnetization in SIT experiment. Jun-lz-L18 concentration, 1310 μM at 15.4°C. (A) Folded form (downfield resonance) initially inverted. (B) Unfolded form (upfield resonance) initially inverted. Solid curves are from global Bayesian analysis of all NMR equilibrium and SIT data, using the equations for the longitudinal component of magnetization vs. time given in Ref. 16 (equations 1–7). Solvent is as in Figure 1.

provide a good fit to the time course of magnetization, as can be judged from Figure 4, and yield the rate constants for both directions. Their ratio provides another experimental value for the equilibrium constant.

Thermodynamic Parameters from NMR and CD

Thermodynamic Parameters from Equilibrium and SIT NMR. Figure 5 shows a van't Hoff plot of the global Bayesian analysis of the combined data sets comprising both equilibrium and dynamic NMR FIDs. The function given by Eq. (3) is shown in Figure 5 as the solid curve, using the thermodynamic parameters from the Bayesian analysis and assuming that $\Delta C^{\infty}_{\mathrm{P,unf}}$ is independent of temperature. The numerical values of the parameters are given in Table I. The inset to Figure 5 shows the distribution of $\Delta H^{\infty}_{\mathrm{unf}}$ (T_0) values obtained from the MCMC procedure. Distributions for the other parameters have a similar appearance.

The self-consistency of the combined equilibrium and SIT data sets with Eq. (3) argues in favor of the assumptions made in our analysis, considering that data were taken by two different NMR methods and range over temperature and concentration. The palpable curvature in the van't Hoff plot and the values in Table I show that there is a substantial positive heat capacity change in unfolding Jun-lz coiled coils, about double the value seen in the case of GCN4-lz.[12]

Thermodynamic Parameters from CD. The Bayesian analysis of our CD data provides values of the standard thermodynamic parameters. These values are displayed in Table I. As can be seen, the values for enthalpy, entropy, and Gibbs energy all agree with those from NMR to better than 5%, in spite of the vast difference in these two experimental techniques. Moreover, the shapes of the CD-derived probability distributions (not shown) are the same as seen for the NMR data (see Figure 5 inset), although the breadths of the distributions are larger for CD. Only the equi-

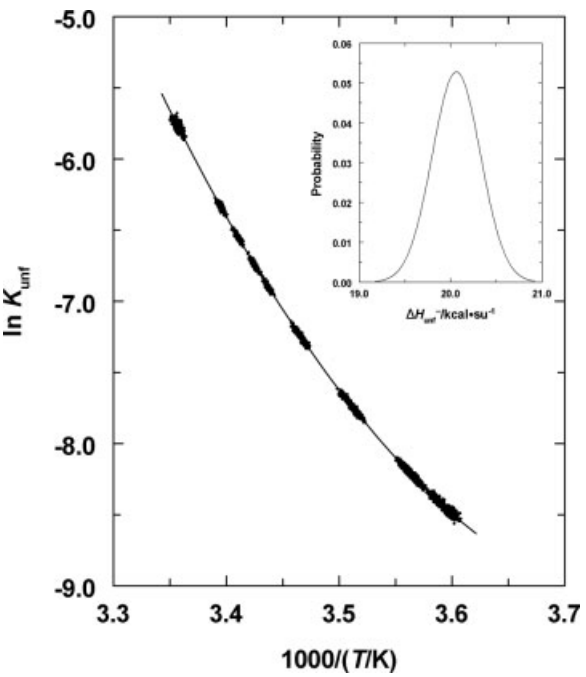

FIGURE 5 van't Hoff plot of unfolding equilibrium results. Points are from global analysis of all NMR equilibrium and SIT data, ranging in concentration from 1310 to 816 μM and in temperature from 1.9 to 25.4°C. For clarity, only 5000 randomly chosen points are shown from the Bayesian blizzard of 65,536 MCMC simulation values. Curve is from Eq. (3) using the parameters from Table I. Inset shows the probability distribution for the standard enthalpy of unfolding at 11.85°C from the Bayesian analysis.

Table I Standard Thermodynamic Parameters for Jun-lz Unfolding[a]

Method	ΔH^{∞}_{unf}[b]	ΔS^{∞}_{unf}[c]	ΔG^{∞}_{unf}[b]	$10^4\,K_{unf}$[d]	$\Delta C^{\infty}_{P,unf}$[c]
NMR	20.06 ± 0.26	55.06 ± 0.92	4.37 ± 0.01	4.48 ± 0.08	847 ± 72
CD	20.86 ± 1.00	57.31 ± 3.36	4.53 ± 0.04	3.36 ± 0.24	463 ± 91

[a] For $F \rightleftharpoons 2U$ in $(NaCl)_{100}(NaPi)_{50}(7.4)$. Error ranges are standard deviations from global Bayesian analysis of combined NMR equilibrium and SIT data or CD data.

[b] kcal su^{-1}; infinitely dilute reference state, molarity units; values for ΔG^{∞}_{unf} and ΔH^{∞}_{unf} apply at $T_0 = 11.85°C$, the transition midpoint at $C_0 = \exp[-\Delta G^{\infty}_{unf}(T_0)/RT_0] = 448\ \mu M$.

[c] cal K^{-1} su^{-1}; infinitely dilute reference state, molarity units; the value given for ΔS^{∞}_{unf} is for $T_0 = 11.85°C$, the transition midpoint at 448 μM. The $\Delta C^{\infty}_{P,unf}$ is assumed independent of T.

[d] Equilibrium constants have no units; here, the units K_{unf} does not have are Mol L^{-1}; the value given is for $T_0 = 11.85°C$, the transition midpoint at 448 μM.

librium constants and the heat capacity changes disagree significantly. The equilibrium constants are exponential in the Gibbs energy, magnifying any differences, and errors in heat capacity, however measured, are invariably large. In view of the difficulties in fitting the CD, as described above, and the larger errors, we consider the values from NMR to be more reliable. In any case, this agreement of NMR and CD results and the lack of any pathology in the probability distributions leaves little doubt that the two different techniques are tracking the same transition. The Bayesian technique is highly sensitive to inaccuracies in the model and to systematic errors in the data. These findings, then, serve to validate our assumption as to the assignment of the observed two NMR resonances to, respectively, spins on coiled-coil dimers and on unfolded monomers.

Kinetic Parameters from SIT NMR

The results of the global Bayesian analysis of all our SIT data are shown in Figure 6 as Arrhenius plots for both the unfolding (A) and folding (B) directions. Insets to each give the probability distribution for $\Delta H^{\ddagger}(T_0)$ from the MCMC procedure. Distributions for other parameters are similar to these in appearance. Numerical values of the kinetic parameters are

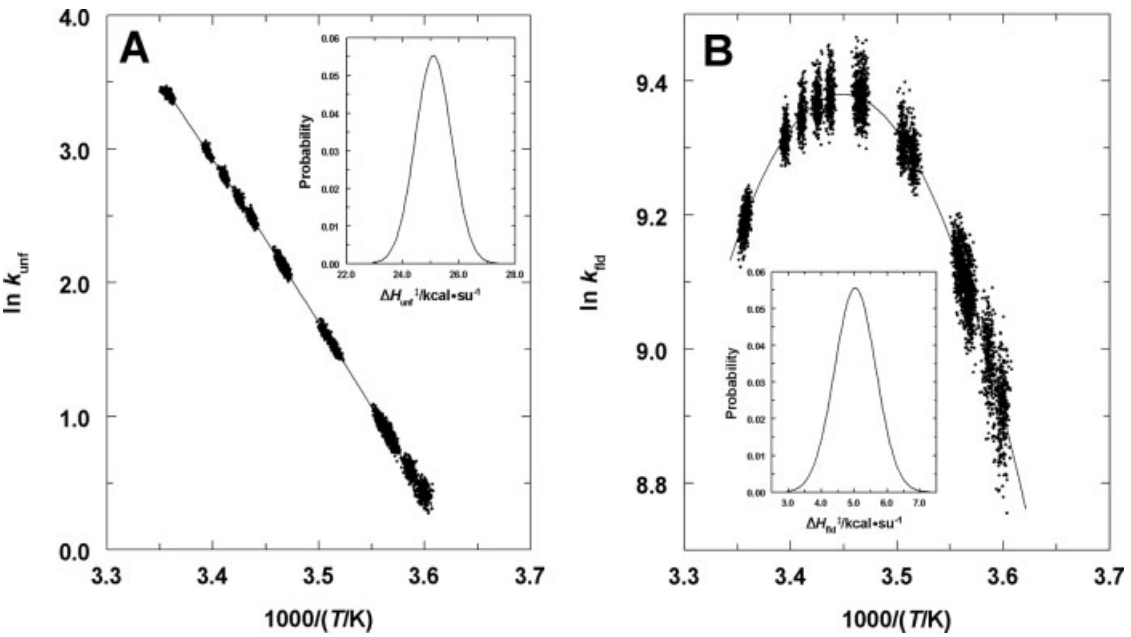

FIGURE 6 Arrhenius plot of the rate constants from the SIT experiments. For clarity, only 5000 randomly chosen points are shown from the Bayesian blizzard of 65,536 MCMC simulation values. Curves are from Eq. (5) using the parameters in Table I. Insets show the probability distributions for the activation enthalpies at 11.85°C from the Bayesian analysis. (A) Unfolding direction. (B) Folding direction.

Table II Kinetic Parameters for Jun-lz-L18 Unfolding and Folding[a]

	k^{b}	$\Delta H^{\ddagger c}$	$\Delta S^{\ddagger d}$	$\Delta G^{\ddagger c}$	$\Delta C_P{}^{\ddagger d}$
unf	4.91 ± 0.12	25.09 ± 0.64	45.44 ± 2.25	12.14 ± 0.01	−170 ± 125
fld	$1.10 \times 10^4 \pm 0.02 \times 10^4$	5.03 ± 0.62	−9.62 ± 2.18	7.77 ± 0.01	−1018 ± 117

[a] For $F \rightleftharpoons A^{\ddagger} \rightleftharpoons 2U$ in $(NaCl)_{100}(NaPi)_{50}(7.4)$ using $Z = 10^{10}$. Error ranges are standard deviations from global Bayesian analysis of NMR SIT data.

[b] s^{-1} for k_{unf}; $M^{-1}\ s^{-1}$ for k_{fld}; values apply at $T_0 = 11.85°C$, the transition midpoint at 448 μM.

[c] kcal su^{-1}; values for $\Delta G^{\ddagger}$ and $\Delta H^{\ddagger}$ apply at $T_0 = 11.85°C$, the transition midpoint at 448 μM.

[d] cal $K^{-1}\ su^{-1}$; values for $\Delta S^{\ddagger}$ apply at $T_0 = 11.85°C$, the transition midpoint at 448 μM. The $\Delta C_P{}^{\ddagger}$ values are assumed independent of T.

given in Table II and are summarized pictorially in the energy level diagrams of Figure 7.

DISCUSSION

Thermodynamic Parameters for Coiled Coils from NMR

The parameters obtained here for Jun-lz are compared with those obtained earlier for GCN4-lz in Table III. To place the values for both peptides on a comparable basis, the GCN4-lz results, which apply at temperatures near 62.7°C, have been corrected to 11.85°C, a temperature more appropriate to the data range encountered in Jun-lz experiments. The correction employs $\Delta C^{\infty}_{P,unf} = 406$ cal $K^{-1}\ su^{-1}$ for the unfolding of GCN4-lz, a result obtained by differential scanning calorimetry.[12]

As Table III shows, the thermodynamic characteristics of the unfolding are vastly different for these two coiled coils. The "instability" of the Jun-lz, as measured by the equilibrium constant for unfolding, is over five orders of magnitude larger than the value for GCN4-lz. The difference cannot be explained by the residues in the *d* heptad position, because the Jun-lz leucine zipper has five at its *d* sites, whereas GCN4-lz has only four, its last such site being an arginine. Furthermore, each peptide possesses an essential dimer-favoring asparagine in a centrally located *a* heptad position.[5,8] However, the other core *a* positions may favor the structured form more in GCN4-lz, which has three valines and a methionine, whereas Jun-lz displays only two valines, an isoleucine, and a lesser hydrophobe in alanine. Moreover, the canonical interstrand salt interactions between a given *e* residue and the *g* of the prior heptad are totally absent in Jun-lz. Whether it is these differences that explain the vast difference in stability cannot be known for certain without further studies of specific mutants.

At any rate, it is clear from Table III that the difference in the standard Gibbs energy of unfolding, the ultimate source of the stabilities, is primarily caused by the difference in the enthalpy rather than the entropy of unfolding the two peptides. All enthalpies and entropies are positive, so the former prevents, while the latter drives, unfolding. However, at 11.85°C, the enthalpy makes twice the contribution to the Gibbs energy difference as the entropy does. Apparently, it is the unfavorable energy of unfolding that is mostly responsible for the difference in instability of the two peptides. Although the entropy of unfolding is larger for GCN4-lz, it is not nearly large enough to compensate for the great increase in enthalpy as one goes from Jun-lz to GCN4-lz. Simula-

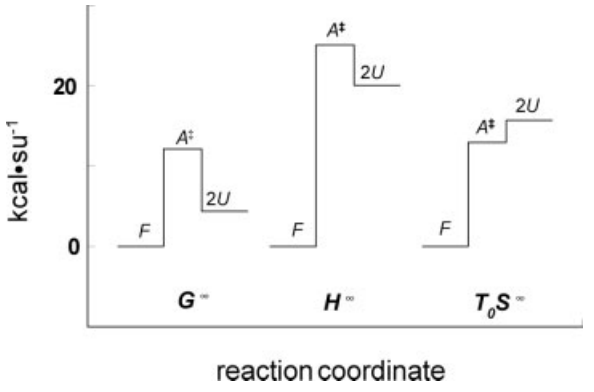

FIGURE 7 Energy level diagram for the processes in stoichiometric Eqs. (1) and (4) at $T_0 = 11.85°C$.

Table III Jun-lz vs. GCN4-lz at T_0 = 285 K: Thermodynamic Parameters[a]

	$\Delta H^{\infty b}_{unf}$	$T_0\ \Delta S^{\infty b}_{unf}$	$\Delta G^{\infty b}_{unf}$	$10^7\ K_{unf}{}^{c}$
GCN4-lz	34.10	22.80	11.30	0.0216
Jun-lz	20.06	15.69	4.37	4480
Difference	14.04	7.11	6.93	

[a] From Table I for Jun-lz; From Table III of Ref. 13 for GCN4-lz using $\Delta C^{\infty}_P = 406$ cal $K^{-1}\ su^{-1}$, the value from Ref. 12.

[b] kcal su^{-1}.

[c] Equilibrium constants have no units; here, the units K_{unf} does not have are Mol L^{-1}.

tions may serve to clarify these differences in more atomic detail.

It is also remarkable that the heat capacity difference between the two peptides is also large, the value for Jun-lz being double that for GCN4-lz. As noted above, this large heat capacity increase upon unfolding is manifest in the CD unfolding curves of Jun-lz, which tend toward a maximum as T drops toward zero. Extrapolation, using the values in Table I, leads to the prediction that the unfolding equilibrium constant for Jun-lz would reach a minimum near -12°C, leading to the onset of "cold denaturation." The Gibbs energy should have a maximum near -6°C. These temperatures are below the normal range of experiments on aqueous solutions, but are perhaps not totally unachievable. It would be of interest to see if a direct experimental test of this prediction could be devised. Because of its much smaller heat capacity change, the corresponding temperatures for GCN4-lz are totally out of the feasible range, both being below the temperature required for onset of ice formation by homogeneous nucleation.[34]

It is perhaps also of interest to compare the thermodynamic parameters of the two coiled coils at the same stability rather than the same temperature.[35] Such a comparison is readily derived from the values in Table III. To match GCN4-lz's unfolding equilibrium constant to the one Jun-lz manifests at 11.85°C (see Table III), requires for the former a temperature of 64.8°C, where its free energy of unfolding is 5.2 kcal su^{-1}, only 0.80 kcal su^{-1} higher than the one for Jun-lz at 11.85°C. Thus, the huge disparity between the enthalpic and entropic contributions to the free energy shown in Table III for GCN4-lz declines greatly at the more elevated temperature. Indeed, at 64.8°C, GCN4-lz's enthalpic contribution would be 55.6 kcal su^{-1} and its entropic contribution -50.4 kcal su^{-1}. Therefore, the difference between the values for the two peptides in enthalpic (35.5 kcal su^{-1}) and entropic (-34.7 kcal su^{-1}) contributions are, respectively, 2.5 times and 4.9 times those found in Table III, where the two peptides are compared at the same low temperature. As expected, the relative contribution of the entropy increases vastly with temperature.

Kinetic Parameters for Coiled Coils from SIT NMR and Other Techniques

Table II and Figure 7 make clear that both folding and unfolding of Jun-lz are activated processes, requiring surmounting a free energy barrier. The barrier for unfolding is more than half again that for folding, although the latter is substantial. Unfolding is entropy driven, enthalpy opposed in that the enthalpic barrier is cut by half, because of a favorable entropy in reaching the transition state from the folded form. This picture is drastically different in the folding process, which is opposed both by enthalpic and entropic contributions to the free energy barrier.

Although the enthalpic barrier for folding is only about one-fifth of that for unfolding, it is nevertheless significant, being nearly 65% of the total barrier to folding. This substantial contribution of enthalpy to the folding barrier is important in the development of an accurate physical picture of the folding of coiled coils. One of the most significant ideas that has been proposed holds that the transition state ensemble comprises dimers in which two unfolded chains, with a small amount of perhaps transient local helix, undergo a simple search of one nucleating segment for its counterpart on the other chain.[36] In that picture, the activation should be purely entropic. In view of the results of Table II and Figure 7, this cannot be the case for Jun-lz, and therefore is not a view of coiled-coil folding that passes muster as a general paradigm.

It should be emphasized that our results do *not* rule out the nucleation-condensation model in general, but only that version of it that posits a simple, i.e., purely entropic, search as needed for the two colliding chains to reach the transition state. Our data require energetic as well as entropic barriers, effects easily accommodated in the more general model.

The changes in heat capacity displayed in Table II for the activation steps for unfolding and folding are also of significance. The value for unfolding is within experimental error of zero, but the one for folding is extremely large, so large that a distinct maximum appears in the folding rate constant near 17°C (Figure 6B). Although it has become part of the conventional wisdom of molecular biophysics to interpret heat capacity changes entirely in terms of exposure of hydrophobic groups to water, this effort is far more difficult than it may appear from the number of examples in the literature. Moreover, recent examination of processes involving polar groups strongly suggests that they can also be accompanied by substantial heat capacity changes.[37] Some combination of molecular effects leads to our results, but at this point, we cannot say much about the heat capacity that is definitive.

Whatever its molecular causes might be, that virtually the entire heat capacity effect seen in the thermodynamic overall unfolding is due to the folding step has important consequences for our general picture of folding/unfolding in GCN4-lz as well as in Jun-lz.

For some time, there has been a discrepancy in the kinetic parameters for folding in GCN4-lz, as obtained by two different laboratories. On the one hand, the Matthews lab reports values for the rate constants for folding and unfolding in the low-*T* region from chevron analysis.[10,11] Not enough data as a function of *T* was taken at that time to provide the temperature dependence. On the other hand, NMR line-shape analysis in our laboratory provides the rate constants in the high-*T* region where the equilibrium in this very stable coiled coil is observable, and data are sufficient to provide activation enthalpies and entropies, so the high-*T* values were corrected to the low-*T* region for comparison with those from chevron analysis.[13] The results reveal that the rate constants for unfolding from the two labs agree remarkably well, despite the long extrapolation to zero denaturant in the chevron case, but the rate constants for folding disagree markedly.[13] It is significant, however, that neither lab's rate data were precise enough to detect heat capacity effects.

Two developments since this disagreement was first noted now combine to resolve the discrepancy. Subsequent work from the Matthews lab reports not only ample temperature data for the rate constants to establish the enthalpies and entropies (but *not* the heat capacities) of activation for GCN4-lz in the low-*T* regime, but also equilibrium data by differential scanning calorimetry (DSC) in the high-*T* regime.[12] The DSC data provide a good value of 406 ± 89 cal K^{-1} su^{-1} for the overall heat capacity change accompanying the unfolding process.

First, we compare the thermodynamic characteristics of the unfolding transition in GCN4-lz from the DSC results of Ibarra et al. (Ref. 12, Table 1) with those from the NMR line-shape findings of Holtzer et al. (Ref. 13, Table 3). These are very different methods, but both employ the high-*T* regime, near 62.7°C. Both groups find a standard enthalpy change for reaction Eq. (1) of near 54 kcal su^{-1} and a standard entropy change near 145 cal K^{-1} su^{-1}. The agreement is extraordinarily good. Indeed, it strongly suggests that the difference in temperature regimes of the kinetic measurements may be responsible for at least some of the disagreement in the rate constants for folding between the two laboratories, an hypothesis we next explore.

In comparing the kinetic parameters determined in the two laboratories, we first look at the results for the unfolding step. Ibarra et al. report an Eyring activation enthalpy (Ref. 12, Table 4) of 34.6 kcal su^{-1} from stopped-flow experiments around a temperature of about 22°C. As noted above, neither lab was able to obtain sufficiently precise rates to allow determination of heat capacities of activation. The NMR line-shape value of 33.8 kcal su^{-1} (Ref. 13, Table 2), obtained near 62.7°C, agrees virtually quantitatively with the stopped-flow value, in spite of the vast difference in temperature regimes of the two measurements. The activation entropies are also in agreement, once one corrects for the differing values of the pre-exponential factor, *Z*, used by the two laboratories.

Apparently, then, one need not assume any heat capacity of activation for the unfolding step. This implies that the total DSC-observed heat capacity change for overall unfolding can be ascribed to the folding kinetic step, because the overall heat capacity change in unfolding must be given by the activation heat capacity change for unfolding minus that for folding. This, in turn, allows us to adjust the kinetic parameters governing the folding rate taken in one temperature regime to that from another.

We proceed by determining what value of the activation heat capacity change for folding is required to bring the two measurement sets into agreement. The NMR-observed value of the enthalpy of activation for folding is given as −20.6 kcal su^{-1}, a value that applies near 62.7°C. Correcting this to yield the stopped-flow determined value of +2.20 kcal su^{-1}, which applies near 22.7°C, requires a heat capacity of activation of −570 cal K^{-1} su^{-1}. Ascribing all of the DSC-observed heat capacity change to the folding step suggests a value of −406 ± 89. Therefore, the value required to produce perfect agreement is a bit outside the standard deviation of the measurement, but within the 95% confidence limit (twice the standard deviation). We submit, therefore, that the discrepancy in the folding rate constant between the stopped-flow and the NMR line-shape determinations is caused by a combination of the differing temperature regimes and the existence of a substantial heat capacity of activation. It seems, then, that the finding in Jun-lz, that the vast bulk of the thermodynamic heat capacity change of the unfolding reaction is manifest in the folding transition, is also true for GCN4-lz. Ironically enough, this possibility was rejected earlier[13] as "extremely unlikely."

Finally, it may be useful to itemize features of these conformational transitions that GCN4-lz and Jun-lz have in common, as these may characterize coiled-coil folding in general. Evidently, both folding and unfolding are activated processes with appreciable free-energy barriers. Moreover, in the low-*T* regime, the barrier to folding is enthalpic as well as free energetic. This seems counterintuitive, because the transition state is generally thought to include some native interactions, which would act to make its energy in between that of the folded and unfolded

states. However, desolvation must occur in the process of forming the transition state ensemble from unfolded chains and the stabilizing interactions are doubtless less perfect than in the native state. The dehydration of backbone polar groups and hydrophobic side chains must prevail over the native-like interactions to produce an energy increase.[35] Note that at higher T, if GCN4-lz is any model, the sign of the activation enthalpy for folding becomes negative, so in that regime, at least, the energy of the transition state is indeed between those of folded and unfolded forms.[13] Lastly, the existence of substantial changes in heat capacity in the transition from folded coiled coil to unfolded monomers seems characteristic of both peptides and seems to be largely confined to the change from the transition state ensemble to the unfolded chains.

Mass spectrometry was provided by the Washington University Mass Spectrometry Resource, a National Institutes of Health Research Resource (Grant No. P41RR0954). Peptide syntheses were performed at the Albert Einstein College of Medicine, supported in part by a grant from the Mathers Foundation. One of us (AH) acknowledges the continuing support of the Luftmensch Society. Another of us (KAS) was supported in part by a grant to Washington University from the Howard Hughes Medical Institute through the Undergraduate Biological Sciences Education Program.

REFERENCES

1. Lupas, A. TIBS 1996, 21, 375–382.
2. Crick, F. H. Acta Crystallogr 1953, 6, 689–697.
3. McLachlan, A. D.; Stewart, M. J Mol Biol 1975, 98, 293–304.
4. O'Shea, E. K.; Rutkowski, R.; Kim, P. S. Science 1989, 243, 538–542.
5. O'Shea, E. K.; Klemm, J. D.; Kim, P. S.; Alber, T. Science 1991, 254, 539–544.
6. Harbury, P. B.; Zhang, T.; Kim, P. S.; Alber, T. Science 1993, 262, 1401–1407.
7. Lumb, K. J.; Carr, C. M.; Kim, P. S. Biochemistry 1994, 33, 7361–7367.
8. Lumb, K. J.; Kim, P. S. Biochemistry 1995, 34, 8642–8648.
9. Sosnick, T. R.; Jackson, S.; Wilk, W.; Englander, W.; DeGrado, W. F. Proteins Struct Funct Genet 1996, 24, 427–432.
10. Zitzewitz, J. A.; Bilsel, O.; Luo, J.; Jones, B. E.; Matthews, C. R. Biochemistry 1995, 34, 12812–12819.
11. Zitzewitz, J. A.; Ibarra-Molero, B.; Fishel, D. R.; Terry, K. L.; Matthews, C. R. J Mol Biol 2000, 296, 1105–1116.
12. Ibarra-Molero, B.; Makhatadze, G. I.; Matthews, C. R. Biochemistry 2001, 40, 719–731.
13. Holtzer, M. E.; Bretthorst, G. L.; d'Avignon, D. A.; Angeletti, R. H.; Mints, L.; Holtzer, A. Biophys J 2001, 80, 939–951.
14. O'Shea, E. K.; Rutkowski, R.; Stafford, W. F., III.; Kim, P. S. Science 1989, 245, 646–648.
15. O'Shea, E. K.; Rutkowski, R.; Kim, P. S. Cell 1992, 68, 699–708.
16. d'Avignon, D. A.; Bretthorst, G. L.; Holtzer, M. E.; Holtzer, A. Biophys J 1998, 74, 3190–3197.
17. d'Avignon, D. A.; Bretthorst, G. L.; Holtzer, M. E.; Holtzer, A. Biophys J 1999, 76, 2752–2759.
18. Lovett, E. G.; d'Avignon, D. A.; Holtzer, M. E.; Braswell, E. H.; Zhu, D.; Holtzer, A. Proc Natl Acad Sci USA 1996, 93, 1781–1785.
19. Holtzer, M. E.; Kumar, S.; Holtzer, A.; Crimmins, D. L. Biopolymers 1989, 28, 1597–1612.
20. Edelhoch, H. Biochemistry 1967, 6, 1948–1954.
21. Holtzer, M. E.; Crimmins, D. L.; Holtzer, A. Biopolymers 1995, 35, 125–136.
22. Bretthorst, G. L. In Lecture Notes in Statistics; Berger, J., Fienberg, S., Gani, J., Krickenberg, K., Singer, B., Eds.; Springer-Verlag: New York, 1988.
23. Bretthorst, G. L. J Magn Res 1990, 88, 533–551.
24. Bretthorst, G. L. J Magn Res 1990, 88, 552–570.
25. Bretthorst, G. L. J Magn Res 1990, 88, 571–595.
26. Jaynes, E. T. In Probability Theory—The Logic of Science; Bretthorst, G. L., Ed.; Cambridge University Press: Cambridge, 2003.
27. Metropolis, N.; Rosenbluth, A. W.; Rosenbluth, M. N.; Teller, A. H.; Teller, E. J Chem Phys 1953, 21, 1087–1091.
28. Gilks, W. R.; Richardson, S.; Spiegelhalter, D. J. Markov Chain Monte Carlo in Practice; Chapman & Hall: London, 1996.
29. Neal, R. M. Probabilistic Inference Using Markov Chain Monte Carlo Methods, Technical Report CRG-TR-93-1, Department of Computer Science, University of Toronto, 1993.
30. Holtzer, M. E.; Lovett, E. G.; d'Avignon, D. A.; Holtzer, A. Biophys J 1997, 73, 1031–1041.
31. Dragen, A. I.; Privalov, P. L. J Mol Biol 2002, 321, 891–908.
32. Holtzer, M. E.; Holtzer, A. Biopolymers 1992, 32, 1589–1591.
33. Holtzer, M. E.; Holtzer, A.; Skolnick, J. Macromolecules 1983, 16, 173–180.
34. Fletcher, N. H. The Chemical Physics of Ice; Cambridge University Press: Cambridge, 1970.
35. Liu, Z.; Chan, H. S. J Mol Biol 2005, 349, 872–889.
36. Myers, J. K.; Oas, T. G. J Mol Biol 1999, 289, 205–209.
37. Cooper, A. Biophys Chem 2005, 115, 89–97.

Reviewing Editor: David Wemmer